ResearchGate

See discussions, stats, and author profiles for this publication at: https://www.researchgate.net/publication/231376567

A Combined Multifluid−Population Balance Model for Vertical Gas−Liquid Bubble-Driven Flows Considering Bubble Column Operating Conditions

ARTICLE *in* INDUSTRIAL & ENGINEERING CHEMISTRY RESEARCH · JANUARY 2011

Impact Factor: 2.59 · DOI: 10.1021/ie101664w

CITATIONS
27

READS
45

6 AUTHORS, INCLUDING:

A. K. Nayak
Indian Institute of Technology Roorkee
16 PUBLICATIONS **103** CITATIONS
SEE PROFILE

Carlos Dorao
Norwegian University of Science and Tech…
68 PUBLICATIONS **743** CITATIONS
SEE PROFILE

Available from: A. K. Nayak
Retrieved on: 02 February 2016

A Combined Multifluid-Population Balance Model for Vertical Gas−Liquid Bubble-Driven Flows Considering Bubble Column Operating Conditions

A. K. Nayak,[†] Z. Borka,[†] L. E. Patruno,[†] F. Sporleder,[†] C. A. Dorao,[‡] and H. A. Jakobsen*,[†]

Department of Chemical Engineering, and Department of Energy and Process Engineering, Norwegian University of Science and Technology, NTNU N-7491 Trondheim, Norway

Fluid particle coalescence and breakage phenomena are important for optimal operation of many industrial process units. In particular, in bubble column reactors, the bubble size distribution determines the interfacial momentum, heat, and mass transfer fluxes through the contact area and may thus limit the overall process performance. To elucidate the mechanisms of the coalescence and breakage phenomena, extensive well-planned model-based experimental investigations are required. In addition, a suitable modeling framework considering the microscopic phenomena is needed to interpret the data achieving extended understanding of the important mechanisms, enabling the formulation of more sophisticated mechanistic kernel functions. This article presents a combined multifluid-population balance model for describing the behavior of vertical bubble-driven flows in bubble columns. In the present modeling approach, the Maxwellian average transport equations for the disperse phase are formulated in terms of a density function. The main advantage of this novel modeling concept is that we obtain a set of transport equations expressed in terms of the set of internal coordinates. All the important moments like the void fraction, contact area, Sauter mean diameter, average disperse phase velocity, mean mass, and momentum fluxes, etc., can then be computed from the predicted density function in a post processing procedure. For model validation, the model predictions are compared to experimental data gathered from the literature. The agreement between the available data and the model predictions ais considered very good. It is concluded that the model is a viable tool for parameter fitting of novel coalescence and breakage kernels provided that sufficient experimental data are made available.

1. Introduction

Bubble columns are widely used for carrying out gas−liquid and gas−liquid−solid reactions in a wide variety of industrial applications. The primary advantages of bubble columns are their simple construction due to having no moving parts, high gas−liquid interfacial area, good heat/mass transfer rates between gas and liquid phase, and large liquid holdup, which is favorable for slow liquid-phase reactions (Shah et al.[1]). In bubble columns, bubbles can break and coalesce due to bubble−bubble and bubble−fluid interactions possibly coupled with certain interphase phenomena. In particular, breakage and coalescence events may produce very different bubble size distributions in the columns. This effect may modify the contact area and the interface fluxes. The present model allows for incorporating more detailed empirical information, which may not be available at the present time.

In the previous work by Dorao and Jakobsen,[2,3] a high order method was developed for the solution of the population balance containing convection and breakage terms. Zhu et al.[4] extended the constant density model to a steady-state 1D combined multifluid-PBE model with both breakage and coalescence terms including a disperse phase momentum balance and the corresponding continuity and momentum balances for the liquid phase. In particular, the axial gas velocity was assumed the same for all particle sizes, hence $v_d = v_d(z)$. The model was applied to a dilute vertical gas−liquid pipe flow. In this article, the model of Zhu et al.[4] has been further extended considering a combined multifluid-PBE model with breakage and coalescence kernels, and bubble growth due to the gas expansion induced through a variable density. Moreover, in the present model, the disperse phase velocity is considered a function of size $v_r = v_r(z,\xi)$. The novel model in which $f_d(z,\xi)$ and $v_r(z,\xi)$ are considered size dependent has been applied simulating two-phase bubble column flows, as illustrated in Figure 1. For model validation, the model predictions are compared to experimental data found in the literature. A similar model approach without the growth and coalescence terms, and with different breakage kernel functions, was used by Patruno et al.[5] and Patruno[6] to simulate gas−liquid droplet flows. However, no experimental droplet flow data were utilized for model validation.

2. Governing Equations

The conventional derivation of the combined multifluid-population balance model based on the density function approach is outlined. Two fundamental modeling frameworks have emerged formulating the multiphase model equations, in quite the same way as the kinetic theory of dilute gases and the continuum mechanical theory were proposed deriving the governing conservation equations of fluid mechanics.

A Boltzmann-like equation is used to describe the dispersed phase behavior. The number of entities in the dispersed phase is assumed to be represented by a continuous probability density function $p(\mathbf{r},\xi,\mathbf{c},\Xi,t)$, with $\mathbf{r}$ denoting the spatial coordinates in physical space, ξ a set of properties characterizing the entities (e.g., diameter, volume, mass, composition, etc.), $\mathbf{c}$ the velocity in the spatial coordinates, Ξ the generalized velocity in the internal coordinates, and t the time.

For the sake of simplicity, we introduce a generalized coordinate vector $\mathbf{q}$ and a generalized velocity vector $\mathbf{a}$ like:

$$\mathbf{q} = \{\mathbf{r}\xi\}^T \qquad \mathbf{a} = \{\mathbf{c}\Xi\}^T \tag{1}$$

* To whom correspondence should be addressed. E-mail: hugo.atle.j@chemeng.ntnu.no.
[†] Department of Chemical Engineering.
[‡] Department of Energy and Process Engineering.

10.1021/ie101664w © 2011 American Chemical Society
Published on Web 01/26/2011

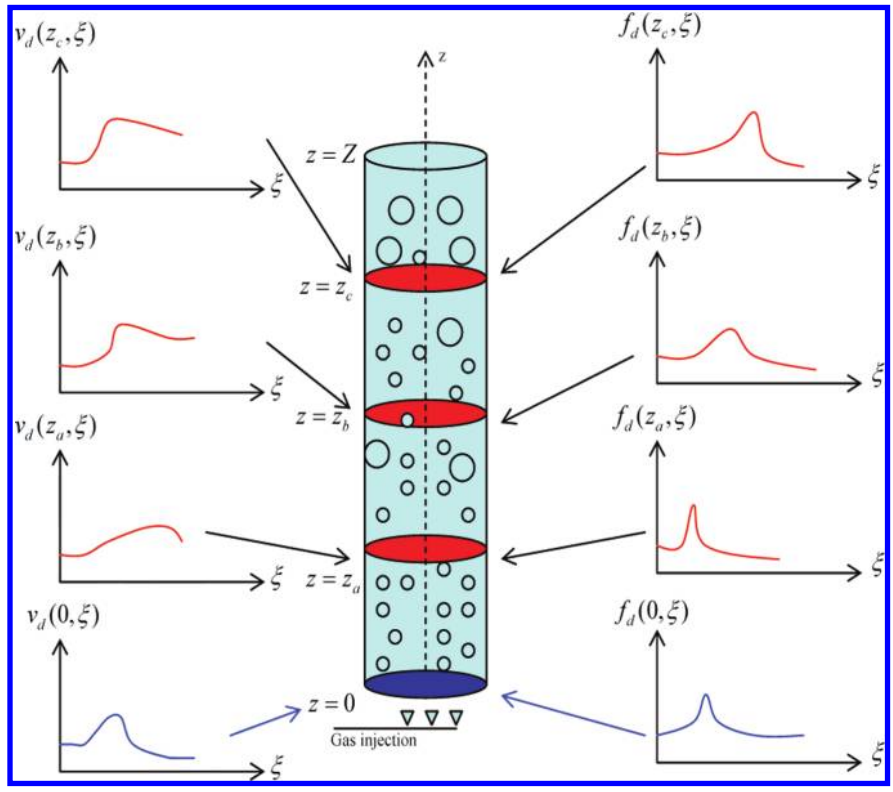

Figure 1. Sketch of a bubble column reactor. Because of the different interaction processes, the distribution of bubbles and the corresponding velocity evolve. The parameter ξ is a characteristic property of the bubble, for example, the bubble volume.

hence the probability density function is represented by $p(\mathbf{q},\mathbf{a},t)$.

The microscopic Boltzmann equation can then be expressed in terms of $p(\mathbf{q},\mathbf{a},t)$, and hence we get:

$$\frac{D_a p}{D_a t} = \frac{\partial p}{\partial t} + \mathbf{a}\cdot\nabla_q p + \mathbf{F}\cdot\nabla_a p = \left(\frac{\partial p}{\partial t}\right)_{\text{collisions}} + S \quad (2)$$

where $\mathbf{F} = \{\mathbf{F}_r\mathbf{F}_\xi\}^T$ is the force term vector per unit mass, which is independent of $\mathbf{a}$. $\mathbf{F}_r$ denotes the force vector per unit mass in physical space, while $\mathbf{F}_\xi$ is the force vector per unit mass in the inner coordinate space. The $\mathbf{F}_r$ term basically contains the gravity, pressure, and drag forces per unit mass, whereas the $\mathbf{F}_\xi$ term represents physical forces per unit mass induced by magnetic or electrical fields. The latter type of forces is not a function of the particle velocity c_i, and thus these terms vanish in the present model as we did not include the particle electrical charge and magnetic properties as internal coordinates. $\nabla_q = (\partial)/(\partial\mathbf{q}) = ((\partial)/(\partial r_1), (\partial)/(\partial r_2), ..., (\partial)/(\partial r_N), (\partial)/(\partial\xi_1), (\partial)/(\partial\xi_2), ..., (\partial)/(\partial\xi_N))$ denote the gradients in the coordinate space, and $\nabla_a = (\partial)/(\partial\mathbf{a}) = ((\partial)/(\partial c_1), (\partial)/(\partial c_2), ..., (\partial)/(\partial c_N), (\partial)/(\partial\Xi_1), (\partial)/(\partial\Xi_2), ..., (\partial)/(\partial\Xi_N))$ represent the gradients in velocity space. The collision source term $((\partial p)/(\partial t))_{\text{collisions}}$ represents the effects of the generalized collisions between the entities. S is a generalized source term that is independent of the collisions.

We may now introduce a generalized property $\psi(\mathbf{q},\mathbf{a},t)$ having velocity in the interval $(\mathbf{a},\mathbf{a}+\mathrm{d}\mathbf{a})$ with position in the interval $(\mathbf{q},\mathbf{q}+\mathrm{d}\mathbf{q})$ within the time period $[t,t+\mathrm{d}t]$ to establish a relation with the variable $p(\mathbf{q},\mathbf{a},t)$. The Maxwellian average of ψ is:

$$\langle\psi\rangle_M(\mathbf{q},t) = \frac{1}{f(\mathbf{q},t)}\int_{-\infty}^{+\infty} p(\mathbf{q},\mathbf{a},t)\psi(\mathbf{q},\mathbf{a},t)\,\mathrm{d}\mathbf{a} \quad (3)$$

The number density $f(\mathbf{q},t)$ denotes the macroscopic property that is obtained by integrating $p(\mathbf{q},\mathbf{a},t)$ over the whole velocity space:

$$f(\mathbf{q},t) = \int_{-\infty}^{+\infty} p(\mathbf{q},\mathbf{a},t)\,\mathrm{d}\mathbf{a} \quad (4)$$

The number density represents the number of entities per unit volume at the position between $[\mathbf{q},\mathbf{q}+\mathrm{d}\mathbf{q}]$ within the time period $[t,t+\mathrm{d}t]$.

The mean velocity $\mathbf{v}(\mathbf{q},t) = \{\langle c\rangle\langle\Xi\rangle\}^T$ is defined by the Maxwellian average of $\mathbf{a}$:

$$\mathbf{v}(\mathbf{q},t) = \langle\mathbf{a}\rangle_M = \frac{1}{f(\mathbf{q},t)}\int_{-\infty}^{+\infty}\mathbf{a}p(\mathbf{q},\mathbf{a},t)\,\mathrm{d}\mathbf{a} \quad (5)$$

Multiplying eq 2 by the property $\psi(\mathbf{q},\mathbf{a},t)$ and integrating over the velocity space, we get:

$$\int_{-\infty}^{+\infty}\frac{D_a p}{D_a t}\psi\,\mathrm{d}\mathbf{a} = \int_{-\infty}^{+\infty}\left(\frac{\partial p}{\partial t}\right)_{\text{collisions}}\psi\,\mathrm{d}\mathbf{a} + \int_{-\infty}^{+\infty} S\psi\,\mathrm{d}\mathbf{a} = J(\psi) \quad (6)$$

where

$$\int_{-\infty}^{+\infty}\frac{D_a p}{D_a t}\psi\,\mathrm{d}\mathbf{a} = \int_{-\infty}^{+\infty}\frac{\partial p}{\partial t}\psi\,\mathrm{d}\mathbf{a} + \int_{-\infty}^{+\infty}\mathbf{a}\cdot\frac{\partial p}{\partial\mathbf{q}}\psi\,\mathrm{d}\mathbf{a} + \int_{-\infty}^{+\infty}\mathbf{F}\cdot\frac{\partial p}{\partial\mathbf{a}}\psi\,\mathrm{d}\mathbf{a} \quad (7)$$

The first term on the right-hand side of eq 7 can be written as

$$\int_{-\infty}^{+\infty}\frac{\partial p}{\partial t}\psi\,\mathrm{d}\mathbf{a} = \int_{-\infty}^{+\infty}\left[\frac{\partial}{\partial t}(p\psi) - p\frac{\partial\psi}{\partial t}\right]\mathrm{d}\mathbf{a} \quad (8)$$

in which we have used the product rule:

$$\frac{\partial}{\partial t}(p\psi) = p\frac{\partial\psi}{\partial t} + \psi\frac{\partial p}{\partial t} \quad (9)$$

We can rewrite the last two terms of eq 8 as

$$\int_{-\infty}^{+\infty} \frac{\partial p}{\partial t}\psi \, \mathrm{d}\mathbf{a} = \frac{\partial}{\partial t}\int_{-\infty}^{+\infty} p\psi \, \mathrm{d}\mathbf{a} - \int_{-\infty}^{+\infty} p\frac{\partial \psi}{\partial t} \, \mathrm{d}\mathbf{a} = \frac{\partial}{\partial t}(f\langle\psi\rangle) - f\left\langle\frac{\partial \psi}{\partial t}\right\rangle_M \quad (10)$$

The second term on the right-hand side of eq 7 can also be rewritten by use of the product rule, and because **q** and **a** are independent coordinates, the result reduces to:

$$\begin{aligned}\int_{-\infty}^{+\infty} \mathbf{a}\cdot\frac{\partial p}{\partial \mathbf{q}}\psi \, \mathrm{d}\mathbf{a} &= \int_{-\infty}^{+\infty}\left[\frac{\partial}{\partial \mathbf{q}}\cdot(p\mathbf{a}\psi) - p\mathbf{a}\cdot\frac{\partial \psi}{\partial \mathbf{q}} - p\psi\cdot\frac{\partial \mathbf{a}}{\partial \mathbf{q}}\right]\mathrm{d}\mathbf{a} \\ &= \frac{\partial}{\partial \mathbf{q}}\cdot\int_{-\infty}^{+\infty}(p\mathbf{a}\psi)\,\mathrm{d}\mathbf{a} - \int_{-\infty}^{+\infty} p\mathbf{a}\cdot\frac{\partial \psi}{\partial \mathbf{q}}\,\mathrm{d}\mathbf{a} \\ &= \frac{\partial}{\partial \mathbf{q}}\cdot(f\langle\mathbf{a}\psi\rangle_M) - f\left\langle\mathbf{a}\cdot\frac{\partial \psi}{\partial \mathbf{q}}\right\rangle_M\end{aligned} \quad (11)$$

Applying the product rule on the third term on the right-hand side of eq 7, and considering that **F** is independent of the velocity **a** and that $p \to 0$ as $\mathbf{a} \to \pm\infty$, the term can be rewritten like:

$$\begin{aligned}\int_{-\infty}^{+\infty} \mathbf{F}\cdot\frac{\partial p}{\partial \mathbf{a}}\psi \, \mathrm{d}\mathbf{a} &= \int_{-\infty}^{+\infty}\left[\frac{\partial}{\partial \mathbf{a}}\cdot(p\mathbf{F}\psi) - p\mathbf{F}\cdot\frac{\partial \psi}{\partial \mathbf{a}} - p\psi\frac{\partial \mathbf{F}}{\partial \mathbf{a}}\right]\mathrm{d}\mathbf{a} \\ &= \int_{-\infty}^{+\infty}\left[\frac{\partial}{\partial \mathbf{a}}\cdot(p\mathbf{F}\psi) - p\mathbf{F}\cdot\frac{\partial \psi}{\partial \mathbf{a}}\right]\mathrm{d}\mathbf{a} \\ &= p\mathbf{F}\psi\Big|_{a=-\infty}^{a=+\infty} - \mathbf{F}\cdot\int_{-\infty}^{+\infty} p\frac{\partial \psi}{\partial \mathbf{a}}\,\mathrm{d}\mathbf{a} \\ &= -\mathbf{F}\cdot f\left\langle\frac{\partial \psi}{\partial \mathbf{a}}\right\rangle_M\end{aligned} \quad (12)$$

Introducing eqs 10−12 into eq 7, we obtain:

$$\begin{aligned}&\int_{-\infty}^{+\infty} \frac{D_a p}{D_a t}\psi \, \mathrm{d}\mathbf{a} \\ &= \frac{\partial}{\partial t}(f\langle\psi\rangle_M) - f\left\langle\frac{\partial \psi}{\partial t}\right\rangle_M + \frac{\partial}{\partial \mathbf{q}}\cdot(f\langle\mathbf{a}\psi\rangle_M) - f\left\langle\mathbf{a}\cdot\frac{\partial \psi}{\partial \mathbf{q}}\right\rangle_M - \mathbf{F}\cdot f\left\langle\frac{\partial \psi}{\partial \mathbf{a}}\right\rangle_M\end{aligned} \quad (13)$$

We may reorganize the terms and define a short form like:

$$\left\langle\frac{D_a\psi}{D_a t}\right\rangle_M = \left\langle\frac{\partial \psi}{\partial t}\right\rangle_M + \left\langle\mathbf{a}\cdot\frac{\partial \psi}{\partial \mathbf{q}}\right\rangle_M + \mathbf{F}\cdot\left\langle\frac{\partial \psi}{\partial \mathbf{a}}\right\rangle_M \quad (14)$$

Next, the equation of change eq 6 for the Maxwellian average generic property $\langle\psi\rangle_M$ can be written as

$$\frac{\partial}{\partial t}(f\langle\psi\rangle_M) + \frac{\partial}{\partial \mathbf{q}}\cdot(f\langle\mathbf{a}\psi\rangle_M) = f\left\langle\frac{D_a\psi}{D_a t}\right\rangle_M + J(\psi) \quad (15)$$

Distinct from the standard derivation of the moment equations, which are obtained by averaging the Boltzmann-like equation over the velocity space and the internal coordinates in one single operation,[9−11] the present model formulation split the averaging process into two different operators. These two operators are the averaging in the velocity space and the averaging in the inner coordinate space. The main advantage of this novel derivation is that we obtain an intermediate result denoting the moment equations for mass and momentum conservation in terms of the set of internal coordinates ξ. These Maxwellian averaged equations may thus be employed to resolve the inner coordinate space physics provided that a sufficient numerical method is available. Using the weighted residual approach, like the least-squares method, we may solve these equations for the unresolved phenomena, and from the Maxwellian averaged distribution function we may compute any of the moments of the inner coordinates in a post processing procedure. The moments behavior computed from this procedure are of course identical to those calculated from the conventional Maxwellian and inner coordinate space average moment equations, which are the mass and momentum conservation equations for the dispersed phase. The hypothesis is that by investigating the intermediate equations, the microscopic physics like the particle breakage and coalescence processes may be better understood, and thus it might be possible to derive more reliable and predictive models for these processes.

The number density equation of change is found by setting $\psi = 1$ into the generic eq 15, hence:

$$\frac{\partial f(\mathbf{r},\xi,t)}{\partial t} + \nabla_r\cdot(\mathbf{v}_r(\mathbf{r},\xi,t)f(\mathbf{r},\xi,t)) + \nabla_\xi\cdot(\mathbf{v}_\xi(\mathbf{r},\xi,t)f(\mathbf{r},\xi,t)) = J(\mathbf{r},\boldsymbol{\xi},t) \quad (16)$$

Thus, $f(\mathbf{r},\xi,t)\,\mathrm{d}\mathbf{r}\,\mathrm{d}\xi\,\mathrm{d}t$ represents the number of bubbles with internal coordinate between $(\xi,\xi+\mathrm{d}\xi)$, position in the interval $(\mathbf{r},\mathbf{r}+\mathrm{d}\mathbf{r})$, during the time interval $(t,t+\mathrm{d}t)$. $\mathbf{v}_r(\mathbf{r},\xi,t)$ denotes the disperse phase velocity for bubbles with internal coordinates ξ, at the point **r** at time t. $\mathbf{v}_\xi$ represents the bubble velocity in the internal coordinate due to expansion, compression, evaporation, condensation, and nucleation. $J(\mathbf{r},\xi,t)$ is a generalized source term considering phenomena like fluid particle breakage and coalescence induced by particle collision mechanisms and processes that are independent of the collisions.

Considering the bubble diameter property only, and in the absence of phase change, the complete form of eq 16 can be written as

$$\begin{aligned}&\frac{\partial f(\mathbf{r},\xi,t)}{\partial t} + \nabla_r\cdot(\mathbf{v}_r(\mathbf{r},\xi,t)f(\mathbf{r},\xi,t)) + \frac{\partial}{\partial \xi}(v_\xi(\mathbf{r},\xi,t)f(\mathbf{r},\xi,t)) \\ &= -b(\mathbf{r},\xi,t)f(\mathbf{r},\xi,t) + \int_{\xi}^{\xi_{\max}} h_b(\zeta,\xi)b(\mathbf{r},\zeta,t)f(\mathbf{r},\zeta,t)\,\mathrm{d}\zeta \\ &\quad - f(\mathbf{r},\xi,t)\int_{\xi_{\min}}^{(\xi_{\max}^3 - \xi^3 + \xi_{\min}^3)^{1/3}} c(\mathbf{r},\xi,\zeta,t)f(\mathbf{r},\zeta,t)\,\mathrm{d}\zeta \\ &\quad + \frac{\xi^2}{2}\int_{\xi_{\min}}^{\xi} \frac{c(\mathbf{r},\xi^3+\xi_{\min}^3-\zeta^3)^{1/3},\zeta,t)}{(\xi^3+\xi_{\min}^3-\zeta^3)^{2/3}} \times \\ &\quad f(\mathbf{r},\zeta,t)f(\mathbf{r},(\xi^3+\xi_{\min}^3-\zeta^3)^{1/3},t)\,\mathrm{d}\zeta\end{aligned} \quad (17)$$

in which $b(\mathbf{r},\xi,t)$ represents the breakage frequency [1/s], $h_b(\zeta,\xi)$ is the daughter size redistribution function [1/m], $c(\mathbf{r},\xi,\zeta,t)$ is the coalescence frequency [1/s], and ξ is the bubble diameter.

Detailed discussions of the population balance equation can be found in the literature.[7,8,13,15,16] Because of number representation issues, it was found convenient to employ a mass density function f_d [kg/(m^3·m)] rather than the number density function f(lb/m^3·m) in eq 17 and the other gas-phase equations.

The mass density function is defined by:

$$f_d = f\rho_d V(\xi) \quad (18)$$

where $V(\xi) = (\pi)/(6)\xi^3$ is the volume of the bubble with size ξ, and ρ_d is the gas-phase density. Hence, after some manipulations, we achieve:

$$\frac{\partial}{\partial t}(f_d(\mathbf{r},\xi,t)) + \nabla_r\cdot(\mathbf{v}_r(\mathbf{r},\xi,t)f_d(\mathbf{r},\xi,t)) - \frac{f_d(\mathbf{r},\xi,t)}{\rho_d(\mathbf{r},t)}\left(\frac{\partial\rho_d(\mathbf{r},t)}{\partial t} + \mathbf{v}_r(\mathbf{r},\xi,t)\cdot\nabla_r\rho_d(\mathbf{r},t)\right) + \frac{\partial}{\partial\xi}(v_\xi(\mathbf{r},\xi,t)f_d(\mathbf{r},\xi,t)) - \frac{3}{\xi}v_\xi(\mathbf{r},\xi,t)f_d(\mathbf{r},\xi,t) = -b(\mathbf{r},\xi,t)f_d(\mathbf{r},\xi,t) + V(\xi)\int_\xi^{\xi_{max}} h_b(\zeta,\xi)b(\mathbf{r},\zeta,t)\frac{f_d(\mathbf{r},\zeta,t)}{V(\zeta)}\,d\zeta - f_d(\mathbf{r},\xi,t)\int_{\xi_{min}}^{(\xi^3_{max}-\xi^3+\xi^3_{min})^{1/3}} c(\mathbf{r},\xi,\zeta,t)\frac{f_d(\mathbf{r},\zeta,t)}{\rho_d(\mathbf{r},t)V(\zeta)}\,d\zeta + \frac{\xi^2}{2}\int_{\xi_{min}}^{\xi}\frac{c(\mathbf{r},(\xi^3+\xi^3_{min}-\zeta^3)^{1/3},\zeta,t)}{(\xi^3+\xi^3_{min}-\zeta^3)^{2/3}}\frac{f_d(\mathbf{r},(\xi^3+\xi^3_{min}-\zeta^3)^{1/3},t)}{V(\xi+\xi_{min}-\zeta)}\times\frac{f_d(\mathbf{r},\zeta,t)}{\rho_d(\mathbf{r},t)V(\zeta)}\,d\zeta \tag{19}$$

It is noted that a similar equation can be derived more elegantly by setting $\psi = m$ into the generic eq 15.

In the absence of phase change, the bubble mass is conserved along its trajectory. As a consequence, the bubble growth velocity and the gas density variation in space and time are related through:[12]

$$v_\xi(\mathbf{r},\xi,t) = -\frac{\xi}{3\rho_d(\mathbf{r},t)}\left(\frac{\partial\rho_d(\mathbf{r},t)}{\partial t} + v_r(\mathbf{r},\xi,t)\cdot\nabla_r\rho_d(\mathbf{r},t)\right) \tag{20}$$

The fluid particle mass can be defined as:

$$m(\mathbf{r},\xi,t) = V(\xi)\rho_d(\mathbf{r},t) = \frac{1}{6}\pi\xi^3\rho_d(\mathbf{r},t) \tag{21}$$

The volume fraction α_d is defined by the third moment of ξ:

$$\alpha_d(\mathbf{r},t) = \int_0^\infty V(\xi)f(\mathbf{r},\xi,t)\,d\xi = \int_0^\infty \frac{f_d(\mathbf{r},\xi,t)}{\rho_d(\mathbf{r},t)}\,d\xi \tag{22}$$

and the mass weighted macroscopic gas velocity in physical space is defined by the first moment of $\mathbf{v}_r(\mathbf{r},\xi,t)$ as:

$$\mathbf{v}_d(\mathbf{r},t) = \frac{\int_0^\infty \mathbf{v}_r(\mathbf{r},\xi,t)f(\mathbf{r},\xi,t)V(\xi)\rho_d(\mathbf{r},t)\,d\xi}{\int_0^\infty f(\mathbf{r},\xi,t)V(\xi)\rho_d(\mathbf{r},t)\,d\xi} = \frac{\int_0^\infty \mathbf{v}_r(\mathbf{r},\xi,t)f_d(\mathbf{r},\xi,t)\,d\xi}{\alpha_d(\mathbf{r},t)\rho_d(\mathbf{r},t)} \tag{23}$$

The momentum equation is obtained by setting $\psi = m(\mathbf{r},\xi,t)c_i$, with $m(\mathbf{r},\xi,t)$ being the mass of the entities of size ξ. Then, the generic equation 15 reduces to

$$\frac{\partial}{\partial t}(f(\mathbf{r},\xi,t)\langle m(\mathbf{r},\xi,t)c_i\rangle) + \nabla_r\cdot(f(\mathbf{r},\xi,t)\langle\mathbf{c}m(\mathbf{r},\xi,t)c_i\rangle) + \frac{\partial}{\partial\xi}(f(\mathbf{r},\xi,t)\langle\Xi m(\mathbf{r},\xi,t)c_i\rangle) = f(\mathbf{r},\xi,t)\left\langle\frac{D_a}{D_a t}(m(\mathbf{r},\xi,t)c_i)\right\rangle + J(m(\mathbf{r},\xi,t)c_i) \tag{24}$$

Hence, because $m(\mathbf{r},\xi,t)$ is independent of $\mathbf{a}$, eq 24 becomes

$$\frac{\partial}{\partial t}(f(\mathbf{r},\xi,t)\rho_d(\mathbf{r},t)V(\xi)\langle c_i\rangle) + \nabla_r\cdot(f(\mathbf{r},\xi,t)\rho_d(\mathbf{r},t)V(\xi)\langle\mathbf{c}c_i\rangle) + \frac{\partial}{\partial\xi}(f(\mathbf{r},\xi,t)\rho_d(\mathbf{r},t)V(\xi)\langle\Xi c_i\rangle) = f(\mathbf{r},\xi,t)V(\xi)\left(\langle c_i\rangle\frac{\partial\rho_d(\mathbf{r},t)}{\partial t} + \langle\mathbf{c}c_i\rangle\cdot\nabla_r\rho_d(\mathbf{r},t) + \langle\Xi c_i\rangle\rho_d(\mathbf{r},t)\left(\frac{3}{\xi}\right)\right) + J(\mathbf{r},\xi,c_i,t) + F_{r_i}(\mathbf{r},\xi,t)m(\mathbf{r},\xi,t)f(\mathbf{r},\xi,t) \tag{25}$$

Neglecting the covariance terms so that the Maxwellian average of products is approximated by the products of average,[8] the momentum eq 25 can be written as:

$$\frac{\partial}{\partial t}(f(\mathbf{r},\xi,t)\rho_d(\mathbf{r},t)V(\xi)v_{r,i}(\mathbf{r},\xi,t)) + \nabla_r\cdot(f(\mathbf{r},\xi,t)\rho_d(\mathbf{r},t)V(\xi)\mathbf{v}_r(\mathbf{r},\xi,t)v_{r,i}(\mathbf{r},\xi,t)) + \frac{\partial}{\partial\xi}(f(\mathbf{r},\xi,t)\rho_d(\mathbf{r},t)V(\xi)\mathbf{v}_\xi(\mathbf{r},\xi,t)v_{r,i}(\mathbf{r},\xi,t)) = f(\mathbf{r},\xi,t)V(\xi)(v_{r,i}(\mathbf{r},\xi,t)\frac{\partial\rho_d(\mathbf{r},t)}{\partial t} + \mathbf{v}_r(\mathbf{r},\xi,t)v_{r,i}(\mathbf{r},\xi,t)\cdot\nabla_r\rho_d(\mathbf{r},t) + v_\xi(\mathbf{r},\xi,t)v_{r,i}(\mathbf{r},\xi,t)\rho_d(\mathbf{r},t)\left(\frac{3}{\xi}\right)) + J(\mathbf{r},\xi,c_i,t) + F_{r_i}(\mathbf{r},\xi,t)m(\mathbf{r},\xi,t)f(\mathbf{r},\xi,t) \tag{26}$$

Substitution of the number density function f by the mass density function f_d, as defined by eq 18, eq 26 yields:

$$\frac{\partial}{\partial t}(f_d(\mathbf{r},\xi,t)v_{r,i}(\mathbf{r},\xi,t)) + \nabla_r\cdot(f_d(\mathbf{r},\xi,t)\mathbf{v}_r(\mathbf{r},\xi,t)v_{r,i}(\mathbf{r},\xi,t)) + \frac{\partial}{\partial\xi}(f_d(\mathbf{r},\xi,t)v_\xi(\mathbf{r},\xi,t)v_{r,i}(\mathbf{r},\xi,t)) = \frac{f_d(\mathbf{r},\xi,t)}{\rho_d(\mathbf{r},t)}v_{r,i}(\mathbf{r},\xi,t)\left(\frac{\partial\rho_d(\mathbf{r},t)}{\partial t} + \mathbf{v}_r(\mathbf{r},\xi,t)\cdot\nabla_r\rho_d(\mathbf{r},t) + v_\xi(\mathbf{r},\xi,t)\rho_d(\mathbf{r},t)\left(\frac{3}{\xi}\right)\right) + J(\mathbf{r},\xi,c_i,t) + F_{r_i}(\mathbf{r},\xi,t)f_d(\mathbf{r},\xi,t) \tag{27}$$

The $F_{r_i}(\mathbf{r},\xi,t)$ term is approximated as:

$$F_{r_i}(\mathbf{r},\xi,t) = -\frac{1}{\rho_d(\mathbf{r},t)}\frac{\partial p(\mathbf{r},t)}{\partial r_i} + g_i + \frac{f_{drag,i}(\mathbf{r},\xi,t)}{f_d(\mathbf{r},\xi,t)} \tag{28}$$

in which the terms on the right-hand side denote the liquid pressure gradient, the gravity, and the steady drag forces per unit mass, respectively.

Inserting the growth velocity eq 20 at one picked place on the right-hand side and the force eq 28 approximations into eq 27, we get:

$$\frac{\partial}{\partial t}(f_d(\mathbf{r},\xi,t)v_{r,i}(\mathbf{r},\xi,t)) + \nabla_r\cdot(f_d(\mathbf{r},\xi,t)\mathbf{v}_r(\mathbf{r},\xi,t)v_{r,i}(\mathbf{r},\xi,t)) + \frac{\partial}{\partial\xi}(f_d(\mathbf{r},\xi,t)v_\xi(\mathbf{r},\xi,t)v_{r,i}(\mathbf{r},\xi,t)) = J(\mathbf{r},\xi,c_i,t) - \frac{f_d(\mathbf{r},\xi,t)}{\rho_d(\mathbf{r},t)}\frac{\partial p(\mathbf{r},t)}{\partial r_i} + f_d(\mathbf{r},\xi,t)g_i + f_{drag,i}(\mathbf{r},\xi,t) \tag{29}$$

2.1. 1-D Steady-State Disperse Gas-Phase Equations. Considering a cross-sectional area averaging, a 1-D steady-state population balance equation is obtained from eq 19:

$$v_r(z,\xi)\frac{\partial f_d(z,\xi)}{\partial z} + f_d(z,\xi)\frac{\partial v_r(z,\xi)}{\partial z} = \frac{v_r(z,\xi)f_d(z,\xi)}{\rho_d(z)}\frac{\partial \rho_d(z)}{\partial z} + \left\{\frac{3\dot{m}_{mass}(z,\xi)}{\xi} - \frac{\partial \dot{m}_{mass}(z,\xi)}{\partial \xi}\right\} - b(z,\xi)f_d(z,\xi) + V(\xi)\int_{\xi}^{\xi_{max}} h_b(\zeta,\xi)b(z,\zeta)\frac{f_d(z,\zeta)}{V(\zeta)}\,d\zeta - f_d(z,\xi)\int_{\xi_{min}}^{(\xi^3_{max}-\xi^3+\xi^3_{min})^{1/3}} c(z,\xi,\zeta)\frac{f_d(z,\zeta)}{V(\zeta)\rho_d(z)}\,d\zeta + \frac{\xi^2 V(\xi)}{2}\int_{\xi_{min}}^{\xi}\frac{c(z,(\xi^3+\xi^3_{min}-\zeta^3)^{1/3},\zeta)}{(\xi^3+\xi^3_{min}-\zeta^3)^{2/3}}\times \frac{f_d(z,(\xi^3+\xi^3_{min}-\zeta^3)^{1/3})}{V(\xi+\xi_{min}-\zeta)}\frac{f_d(z,\zeta)}{V(\zeta)\rho_d(z)}\,d\zeta \quad (30)$$

together with a consistent momentum equation from eq 29:

$$\frac{\partial}{\partial z}(f_d(z,\xi)v_r(z,\xi)v_r(z,\xi)) = -\frac{\partial}{\partial \xi}(\dot{M}_{momentum}(z,\xi)) + J(z,\xi,c_i) - \frac{f_d(z,\xi)}{\rho_d(z)}\frac{\partial p(z)}{\partial z} + f_d(z,\xi)g + f_{drag}(z,\xi) \quad (31)$$

In these two equations, the mass and momentum fluxes in the property coordinate have been introduced in accordance with the standard notation for practical applications:[13]

$$\dot{m}_{mass} = f_d(z,\xi)v_\xi(z,\xi) \quad (32)$$

and

$$\dot{M}_{momentum}(z,\xi) = f_d(z,\xi)v_\xi(z,\xi)v_r(z,\xi) \quad (33)$$

The volume fraction $\alpha_d(z)$ is computed from eq 22:

$$\alpha_d(z) = \int_0^\infty \frac{f_d(z,\xi)}{\rho_d(z)}\,d\xi \quad (34)$$

The bubble growth velocity is estimated from eq 20 as:

$$v_\xi(z,\xi) = -\frac{\xi}{3\rho_d(z)}\left(v_r(z,\xi)\frac{\partial \rho_d(z)}{\partial z}\right) \quad (35)$$

The disperse phase density is computed from the ideal gas law given by

$$p(z) - \frac{p^0}{\rho_d^0}\rho_d(z) = 0 \quad (36)$$

Moreover, the gas-phase pressure is assumed equal to the liquid-phase pressure: $p = p_g = p_l$. The term f_{drag} is the drag force denoting the momentum gain in the liquid phase due to the retardation of the bubble phase. The drag force is defined as:[5]

$$f_{drag} = -\frac{3}{4}\rho_l\frac{C_D f_d(z,\xi)}{\xi\,\rho_d(z)}|v_r(z,\xi) - v_l(z)|(v_r(z,\xi) - v_l(z)) \quad (37)$$

and the drag coefficient C_D for clean water yields:[18]

$$C_D = \max\left\{\min\left[\frac{16}{Re_p}(1 + 0.15Re_p^{0.687}), \frac{48}{Re_p}\right], \frac{8}{3}\frac{E_0}{E_0+4}\right\} \quad (38)$$

The particle Reynolds number, Re_p, and the Eötvös number, E_0, are defined by:

$$Re_p(z,\xi) = \frac{\rho_l|v_r(z,\xi) - v_l(z)|\xi}{\mu_l} \quad (39)$$

$$E_0 = \frac{g(\rho_l - \rho_g)\xi^2}{\sigma_l} \quad (40)$$

The breakage frequency kernel of Coulaloglou and Tavlarides[19] with the daughter size redistribution function of Konno et al.[21] were used together with the coalescence frequency kernel of Prince and Blanch.[22] The breakage frequency yields:[19]

$$b(\xi) = \frac{k_1\varepsilon^{1/3}}{\xi^{2/3}}\exp\left(-\frac{\sigma_l k_2}{\rho_d\varepsilon^{2/3}\xi^{5/3}}\right) \quad (41)$$

in which k_1 and k_2 are empirical parameters, which depend on the system properties. In this work, the parameter values used are $k_1 = 0.0336s$ and $k_2 = 0.205$.

The average dissipation rate ε is approximated by the ratio of the specific kinetic energy introduced by the gas and the mass of the liquid in the bubble column:

$$\varepsilon = \frac{j_g g\rho_l(1-\alpha)}{\rho_l(1-\alpha)} = j_g g \quad (42)$$

in which g represents the gravitational acceleration, and j_g is the volumetric flux of gas, respectively.

The daughter size redistribution function $h_b(\zeta,\xi)$ of Konno et al.[21] is expressed as:

$$h_b(\zeta,\xi) = \frac{\Gamma(12)}{\Gamma(3)\Gamma(9)\zeta}\left(\frac{\xi}{\zeta}\right)^8\left[1 - \frac{\xi}{\zeta}\right]^2 \quad (43)$$

The coalescence model concept proposed by Prince and Blanch[22] for the rates of bubble coalescence in turbulent gas−liquid dispersions has been adopted. In this modified kernel, the coalescence frequency $c(\xi,\zeta)$ has been defined as the product of an effective swept volume rate $h_c(\xi,\zeta)$ and the coalescence probability $\lambda_c(\xi,\zeta)$ with a prefactor of 0.05, hence:

$$c(\xi,\zeta) = 0.05h_c(\xi,\zeta)\lambda_c(\xi,\zeta) \quad (44)$$

The closures for the effective swept volume rate and the coalescence probability used in this work are based on the assumption that turbulence is the dominant mechanism determining the coalescence frequency. In this case, the swept volume rate is defined as

$$h_c(\xi,\zeta) = \frac{\pi}{4}(\xi+\zeta)^2(\overline{v_t^2(\xi)} + \overline{v_t^2(\zeta)})^{1/2} \quad (45)$$

in which $\overline{v_t^2(\xi)} = \beta(\varepsilon\xi)^{2/3}$ and $\beta \approx 2.0$.

The collision efficiency determines the fraction of bubble collisions that leads to coalescence events. The expression for the dimensionless coalescence efficiency proposed by Prince and Blanch[22] is given by:

$$\lambda_c(\xi,\zeta) = \exp\left[-\frac{\left(\frac{r_c^3(\xi,\zeta)\rho_l}{16\sigma}\right)^{1/2}\varepsilon^{1/3}\ln\frac{h_0}{h_f}}{(r_c(\xi,\zeta))^{2/3}}\right] \quad (46)$$

in which $h_0 = 10^{-4}$ m is the initial film thickness, and $h_f = 10^{-8}$ m is the critical film thickness for rupture. The equivalent radius r_c is approximated by

$$r_c(\xi,\zeta) = \frac{1}{4}\left(\frac{1}{\xi} + \frac{1}{\zeta}\right)^{-1} \quad (47)$$

2.2. 1-D Steady-State Continuous Liquid-Phase Equations. Considering cross-sectional area averaging, and given no source or sink terms for the liquid phase, the liquid continuity equation is given by:[8]

$$\frac{\mathrm{d}}{\mathrm{d}z}[\alpha_\mathrm{l}(z)\rho_\mathrm{l}v_\mathrm{l}(z)] = 0, \text{integrated: } \alpha_\mathrm{l}(z)\rho_\mathrm{l}v_\mathrm{l}(z) = \alpha_\mathrm{l}(z=0)\rho_\mathrm{l}v_\mathrm{l}(z=0) \quad (48)$$

in which $\alpha_\mathrm{l}(z)$ is the liquid-phase volume fraction, ρ_l is the liquid density (assumed constant), and $v_\mathrm{l}(z)$ is the liquid velocity.

The liquid-phase momentum equation is given by:[5]

$$\alpha_\mathrm{l}(z)\rho_\mathrm{l}v_\mathrm{l}(z)\frac{\partial}{\partial z}v_\mathrm{l}(z) = \alpha_\mathrm{l}(z)\left(-\frac{\partial p(z)}{\partial z} - \frac{1}{2}\rho_\mathrm{l}\frac{f_\mathrm{w}(z)}{D}v_\mathrm{l}(z)^2\right) - \int_0^\infty f_\mathrm{drag}(z,\xi)\,\mathrm{d}\xi + \alpha_\mathrm{l}(z)\rho_\mathrm{l}(z)g \quad (49)$$

The terms on the right-hand side represent the pressure gradient, the wall friction, the steady drag force, and the gravity forces per unit volume, respectively. Moreover, $f_\mathrm{w}(z)$ denotes the wall friction factor, and D is the column diameter.

The summation of the phase area fractions must be unity, and hence a compatibility condition is required:

$$\alpha_\mathrm{l}(z) + \alpha_\mathrm{d}(z) = 1 \quad (50)$$

The wall friction factor is calculated as:[20]

$$f_\mathrm{w}(z) = (0.79\ln[Re_\mathrm{l}(z)] - 1.64)^{-2} \quad (51)$$

in which the Reynolds number Re_l is defined like:

$$Re_\mathrm{l}(z) = \frac{\rho_\mathrm{l}(z)v_\mathrm{l}(z)D}{\mu_\mathrm{l}} \quad (52)$$

2.3. Initial Conditions. To solve the given set of hyperbolic equations, suitable initial conditions must be defined.

It is noted that under bubble column operation, the inlet gas and liquid volume fluxes j_l,j_d are normally kept constant at specified values. This means that neither the area fractions nor the local gas- and liquid-phase velocities are known at the inlet, and hence an iterative scheme is defined to compute these variable values from the specified fluxes and an approximate density function as defined below.

Gas Inlet in Property (Size) and Space. The initial conditions for the gas mass density function f_d are specified as:

$$fd(z,\xi_\mathrm{min}) = 0, \quad \forall z \quad (53)$$

and

$$f_\mathrm{d}^*(z=0,\xi) = \frac{\phi(\xi)}{A}\int_{\xi_\mathrm{min}}^{\xi_\mathrm{max}} f_\mathrm{d}^*(z=0,\xi)\,\mathrm{d}\xi = \frac{\phi(\xi)}{A}\alpha_\mathrm{d}^*(z=0)p_\mathrm{d}^*(z=0), \quad \forall\xi \quad (54)$$

in which $\phi(\xi)$ is the Gaussian distribution function,[14] and "*" denotes the previous Pichard iteration variable values. A denotes the area under the $\phi(\xi)$-curve and is used to normalize the distribution function, when the function values at the integral limits do not approach to zero.

It was mentioned above that the initial distribution $f_\mathrm{d}(z = 0,\xi)$ is defined subject to the constraint:

$$v_\mathrm{d}^*(z=0)\alpha_\mathrm{d}^*(z=0) = j_\mathrm{d} \quad (55)$$

The dispersed gas-phase velocity is given by:

$$v_\mathrm{d}^*(z) = \frac{\int_0^\infty f_\mathrm{d}^*(z,\xi)v_\mathrm{r}^*(z,\xi)\,\mathrm{d}\xi}{\int f_\mathrm{d}^*(z,\xi)\,\mathrm{d}\xi} = \frac{\int_0^\infty f_\mathrm{d}^*(z,\xi)v_\mathrm{r}^*(z,\xi)\,\mathrm{d}\xi}{\alpha_\mathrm{d}^*(z)\rho_\mathrm{d}^*(z)} \quad (56)$$

The initial gas bubble phase velocity v_r^* is specified as $v_\mathrm{r}(z, \xi_\mathrm{min}) = 0$, $\forall z$, and the dispersed phase bubble velocity at $z = 0$ is approximated as:

$$v_\mathrm{r}^*(z=0,\xi) = v_\mathrm{l}^*(z=0) + v_\mathrm{d,slip}(\xi) \quad \forall\xi \quad (57)$$

The slip velocity is computed from the relations given by Fan and Tsuchiya:[23]

$$v_\mathrm{d,slip}(\xi) = (v_{\mathrm{b}_1}^{-n} + v_{\mathrm{b}_2}^{-n})^{-1/n} \quad (58)$$

with

$$v_\mathrm{b1} = \frac{\rho_\mathrm{l}g\xi^2}{K_\mathrm{b}\mu\mathrm{l}}; \quad v_\mathrm{b2} = \sqrt{\frac{2\sigma_\mathrm{l}}{\rho_\mathrm{l}\xi} + \frac{g\xi}{2}} \quad (59)$$

where the constant K_b is predefined to be 12, and n is chosen at 0.8.[23]

A fixed liquid inlet volume flux j_l is specified. The liquid area fraction is computed from the gas area fraction α_d using the compatibility condition (50):

$$\alpha_\mathrm{l}^*(z=0) = 1 - \alpha_\mathrm{d}^*(z=0) \quad (60)$$

The liquid inlet velocity can then be computed from the inlet liquid flux:

$$v_\mathrm{l}^*(z=0) = \frac{j_\mathrm{l}}{\alpha_\mathrm{l}^*(z=0)} \quad (61)$$

A fixed outlet pressure p is specified.

2.4. The First Guesses of the Variable Values for the Iteration Process. The pressure, gas area fraction, and density profiles have been estimated as follows:

Pressure:

$$p(z) = p(z=z_\mathrm{max}) + \rho_\mathrm{l}(z)g(z_\mathrm{max} - z) \quad (62)$$

considering the pressure distribution in a column filled with liquid only.

Density:

$$\rho_\mathrm{g}(z) = \frac{p(z)M}{RT} \quad (63)$$

by use of the ideal gas law, where R is the universal gas constant, and T is the temperature.

Gas area fraction:

$$\alpha_\mathrm{d}(z) = \alpha_\mathrm{d}(z=0) \quad (64)$$

the void profile is considered constant all over the domain.

Based on the initial distribution for $f_\mathrm{d}(z = 0,\xi)$ estimated as:

$$f_\mathrm{d}^*(z=0,\xi) = \frac{\phi\xi}{A}\int f_\mathrm{d}^*(z=0,\xi)\,\mathrm{d}\xi = \frac{\phi\xi}{A}\alpha_\mathrm{d}^*(z=0)\rho_\mathrm{d}^*(z=0), \quad \forall\xi \quad (65)$$

the variable guess initialization is performed by extending the initial conditions to the whole domain.

3. Numerical Method

The set of governing equations are solved by the spectral least-squares method.[2−6,8,17,24,25] To simplify the notation, we can define the problem operator $\mathscr{L}$ such that:

$$\mathscr{L}\boldsymbol{f}(z,\xi) = \boldsymbol{g}(z,\xi), \text{ in } \Omega = [\xi_{\min}, \xi_{\max}] \times [z_{\min}, z_{\max}] \in \mathbb{R}^2 \tag{66}$$

$$\mathscr{B}_0\boldsymbol{f}(z,\xi) = \boldsymbol{f}_0(z,\xi), \text{ on } \Gamma_0 \tag{67}$$

in which $\boldsymbol{f}^T = (v_l, p, f_d, \dot{m}_{\text{mass}}, v_r, \dot{M}_{\text{momentum}}, \alpha_d, \rho_d, v_\xi)$ is the vector of unknown functions. The $\dot{m}_{\text{mass}} = f_d v_\xi$ and $\dot{M}_{\text{momentum}} = f_d v_\xi v_r$ are the fluxes of mass eq 32 and momentum eq 33 in the ξ-coordinate, respectively. $\mathscr{B}_0$ is the algebraic boundary operators. To handle the nonlinearity, the $\mathscr{L}$-operator is linearized to $\mathscr{L}^*$ to implement a Picard iteration solution technique. Hence, the system of equations can be expressed as $A^*\boldsymbol{f} = g^*$ in which the asterisk indicates a linearized form. For the actual problem, the operators are redefined as

$$\mathscr{L}^* = \begin{bmatrix}
\rho_l(1-\alpha_d^*)(\bullet) & 0 & 0 & 0 & 0 & 0 & 0 & 0 & 0 \\
\rho_l(1-\alpha_d^*)v_l^*\dfrac{d}{dz}(\bullet) & (1-\alpha_d^*)\dfrac{d}{dz}(\bullet) & 0 & 0 & 0 & 0 & 0 & 0 & 0 \\
0 & 0 & \rho_d^* v_r^* \dfrac{d}{dz}(\bullet) - \rho_d^*\mathscr{B}^* - \rho_d^*\mathscr{C}^* & 0 & \rho_d^* f_d^* \dfrac{d}{dz}(\bullet) & 0 & 0 & -f_d^* v_r^* \dfrac{d}{dz}(\bullet) & 0 \\
0 & 0 & 0 & 1(\bullet) & 0 & 0 & 0 & 0 & 0 \\
-k_{\text{drag}}^* f_d^*(\bullet) & f_d^*\dfrac{d}{dz}(\bullet) & v_r^* v_r^* \dfrac{d}{dz}(\bullet) + g(\bullet) & 0 & k_{\text{drag}}^* f_d^*(\bullet) & 0 & 0 & 0 & 0 \\
0 & 0 & 0 & 0 & 0 & 1(\bullet) & 0 & 0 & 0 \\
0 & 0 & 0 & 0 & 0 & 0 & 1(\bullet) & 0 & 0 \\
0 & 0 & 0 & 0 & 0 & 0 & 0 & 1(\bullet) & 0 \\
0 & 0 & 0 & 0 & 0 & 0 & 0 & 0 & \rho_d^*(\bullet)
\end{bmatrix} \tag{68}$$

where $\mathscr{B}^* = \mathscr{L}_{\mathscr{B}}^*$ is the net breakage source term operator and $* = \mathscr{L}^*$ is the net coalescence source term operator. Because of the scaling problem, the drag term is divided into two terms, one kept inside $\mathscr{L}^*$ and the other included in the source term g^*.

The linearized source vector is defined as as

$$g^* = \begin{bmatrix}
\rho_l(1.0 - \alpha_d^*(z=0))v_l^*(z=0) \\
-\dfrac{1}{2}(1-\alpha_d^*)\dfrac{f_w^*}{D}\rho_l v_l^* - (1-\alpha_d^*)\rho_l g + \int f_{\text{drag}}^*\, d\xi \\
\dfrac{3}{\xi}\rho_d^*\dot{m}_{\text{mass}}^* - \rho_d^*\dfrac{d}{d\xi}(\dot{m}_{\text{mass}}^*) \\
f_d^* v_\xi^* \\
-2f_r^* v_r^* \dfrac{d}{dz}(v_r^*) \\
f_d^* v_\xi^* v_r^* \\
\int \dfrac{f_d^*}{\rho_d^*}\, d\xi \\
p^* \\
-\dfrac{\left(\xi - \dfrac{\xi_{\min}}{\xi_{\max}}\right)}{3} v_r^* \dfrac{d}{dz}(\rho_d^*)
\end{bmatrix} \tag{69}$$

Because the problem is nonlinear, we have to make iterations to get a converged solution. To access the convergence of the model, we define two convergence error measures as:

$$\varepsilon_{L2} = \sqrt{\int_\Omega R^{*2}\, d\Omega} = \sqrt{\int_\Omega (\mathscr{L}^* f_N - g^*)^2\, d\Omega} \tag{70}$$

$$\varepsilon_{\text{iteration}} = \sqrt{\int_\Omega (f_N^{\text{it}} - f_N^{\text{it}-1})^2\, d\Omega} \tag{71}$$

with ε_{L2} the error related to the least-squares method, $\varepsilon_{\text{iteration}}$ the error related to the Picard iteration technique, $\mathscr{L}^*$ the linearized integro-differential operator, and g^* the linearized source term. Moreover, underrelaxation of the iteration process was required and defined as: $f_N = \alpha f_N^{\text{it}-1} + (1-\alpha) f_N^{\text{it}}$, with a typical underrelaxation parameter value of $\alpha = 0.6$. In our computations, we have considered the following convergence criteria limits: $\varepsilon_{L2} \le 10^{-5}$ and $\varepsilon_{\text{iteration}} \le 10^{-9}$.

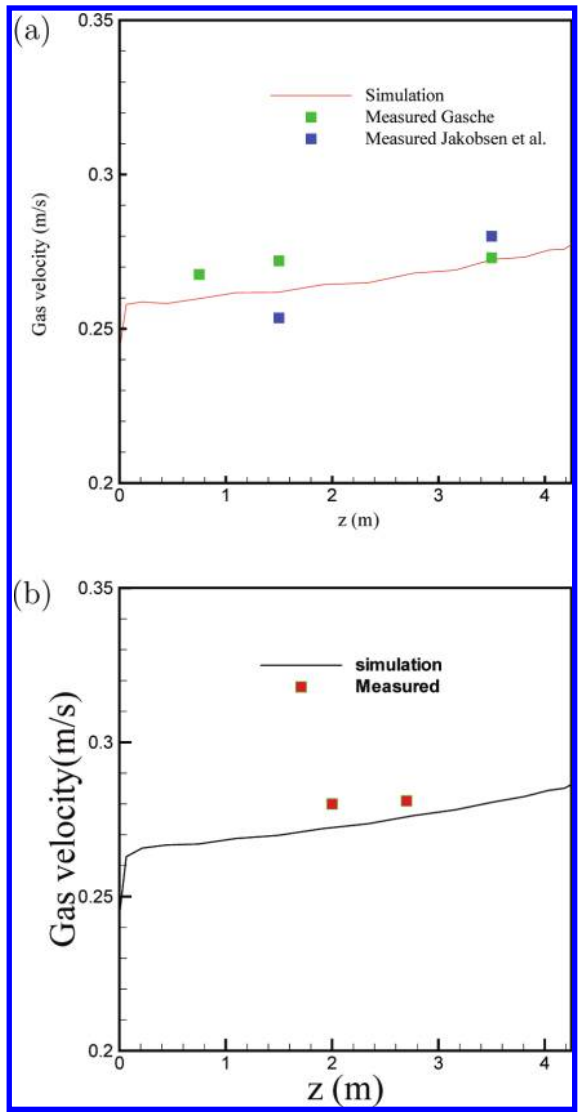

Figure 2. Model validation: (a) A comparison between the predicted gas velocity profile and the experimental data obtained from Jakobsen et al.[27] and Gasche[29] for gas flux $j_d = 0.04$ m/s. (b) A comparison between the predicted profile and the experimental data obtained from Jakobsen[28] for gas flux $j_d = 0.08$ m/s.

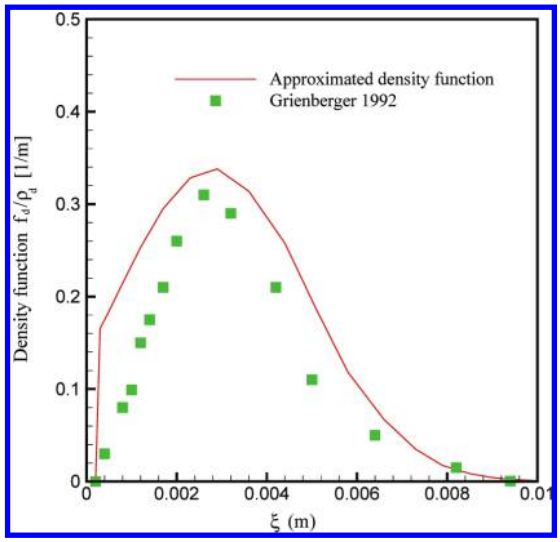

Figure 3. Fit of the density function, that is, $f_d(z,\xi)/\rho_d(z)$ [1/m], to the experimental data obtained from Grienberger[30] with gas flux $j_d = 0.02$ m/s over the ξ property domain.

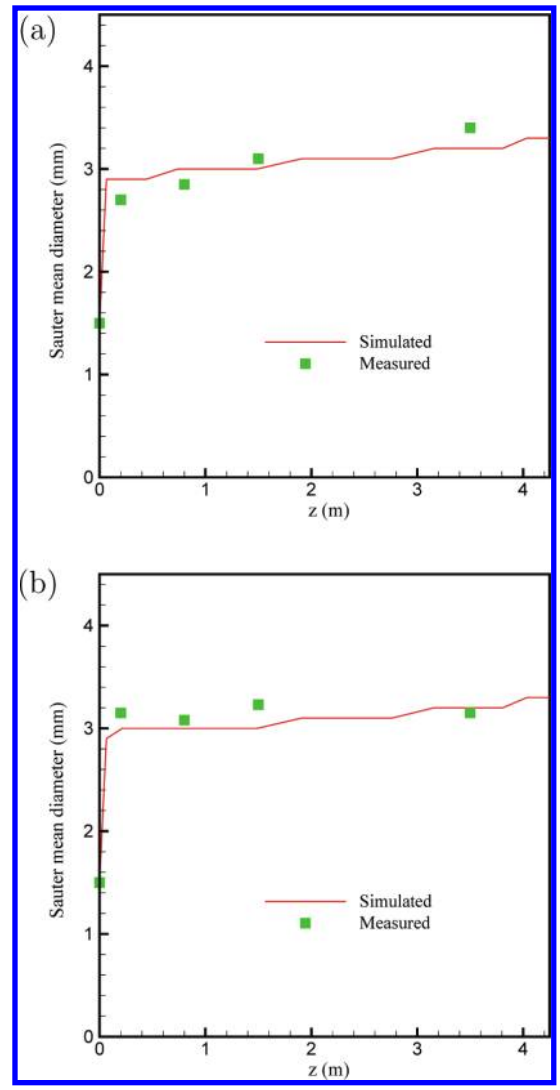

Figure 4. Sauter mean diameter predictions as compared to the experimental results obtained by Jakobsen et al.:[27] (a) with gas flux $j_d = 0.02$ m/s, (b) with gas flux $j_d = 0.08$ m/s.

4. Results and Discussion

The general parametric values used for these simulations are pipe length 4.25 m, diameter 29 cm, bubble diameter sizes between 0.0005 m and 0.015 m, and in all cases the liquid flux is $j_l = 0.01$ m/s. It is noted that the experimental raw data used were measured at a limited number of positions over the radial dimension of the column and at a few axial levels, as no cross-sectional average data sets are reported in the literature. The 1D model results have thus been compared to area-averaged data computed from the raw data over the radial dimension. No detailed error analysis of the experimental data is provided in the literature.

The results for the gas velocity are presented in Figure 2 for different gas flux values. In Figure 2a, we have presented a gas velocity comparison with the experimental analyzes reported by Jakobsen et al.[27] and Gasche[29] for a gas flux $j_d = 0.04$ m/s. It is seen that the agreement between the experimental data and the numerical solution is very good. In Figure 2b, we have presented a gas velocity comparison between the simulated profiles and the experimental data presented by Jakobsen[28] for a gas flux $j_d = 0.08$ m/s. The agreement between the experimental data and the model prediction is very good for this case too. Figure 3 shows the approximate inlet values of the density

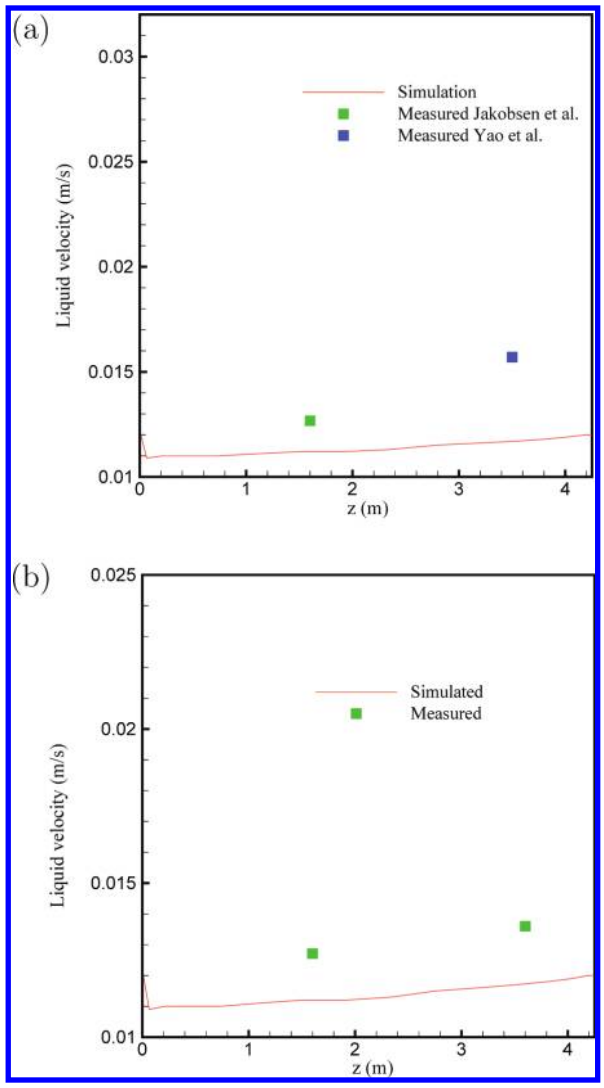

Figure 5. Liquid velocity predictions as compared to (a) the experimental data obtained from Jakobsen et al.[27] and Yao et al.[31] with gas flux j_d = 0.04 m/s, and (b) the experimental data obtained from Jakobsen[28] with gas flux j_d = 0.08 m/s.

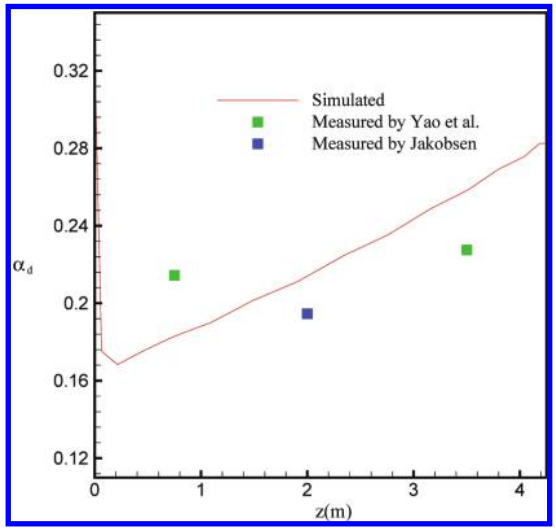

Figure 6. The gas area fraction profile predicted with a gas flux j_d = 0.08 m/s is compared to the corresponding experimental data reported by Jakobsen[28] and Yao et al.[31]

function f_d over the ξ-property domain. The approximate density function was tuned to the experimental data given by Grienberger.[30] The same density function approximation was used for all cases, as no more suitable data are available. The Sauter mean diameter can be computed as:

$$d_{32}(z) = \frac{\int_0^\infty f_d(z,\xi)\,d\xi}{\int_0^\infty \frac{f_d(z,\xi)}{\xi}\,d\xi} \tag{72}$$

Figure 4a,b shows the Sauter mean diameter profiles in the axial direction of the column for two different gas flux values (i.e., j_d = 0.02 and 0.08 m/s, respectively). In both cases, the predicted results are in good agreement with the experimental data. In Figure 4a, the data for j_d = 0.02 m/s are used as no data were found for the 0.04 m/s case. In Figure 5 a, we have presented a comparison of the simulated liquid velocity results and the experimental data reported by Jakobsen et al.[27] and Yao et al.[31] for a gas flux j_d = 0.04 m/s, and in Figure 5b the corresponding data by Jakobsen[28] for a gas flux j_d = 0.08 m/s are compared. The agreement between the simulated profiles and the average experimental data is fair. However, these data show that the deviation between the numerical results and the

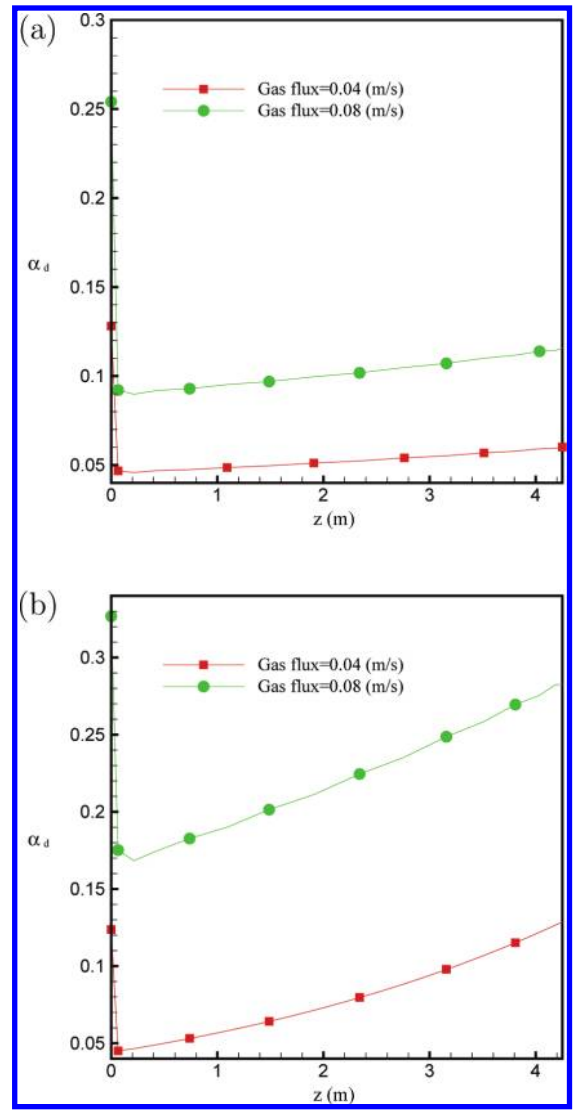

Figure 7. Void fraction plotted as a function of z for two different gas flux values, (a) without breakage and coalescence terms, and (b) with breakage and coalescence terms.

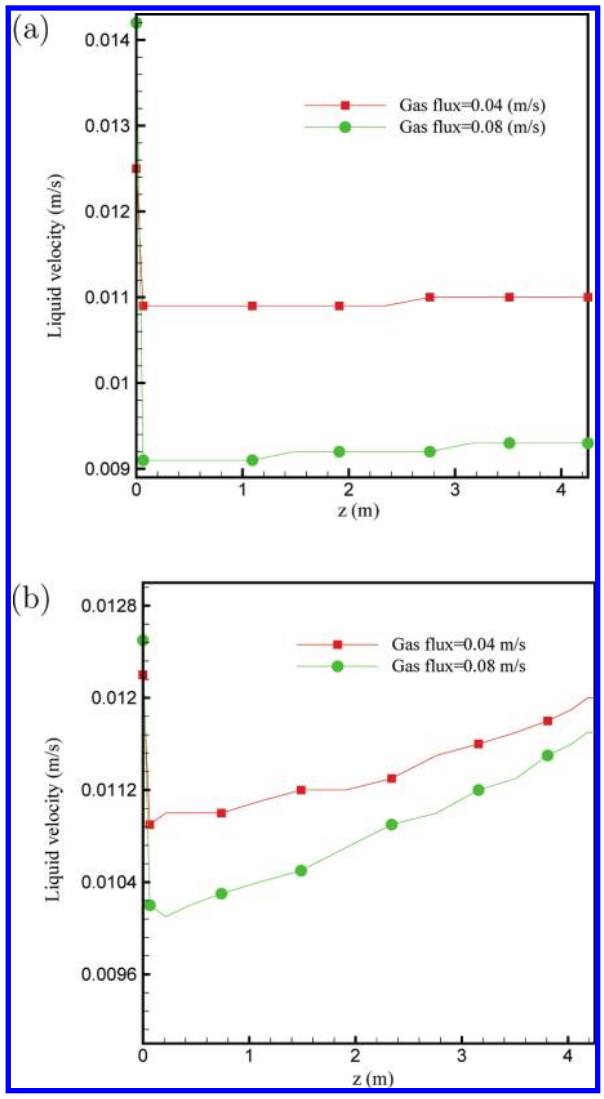

Figure 8. Liquid velocity plotted as a function of z for two different gas flux values, (a) without breakage and coalescence terms, and (b) with breakage and coalescence terms.

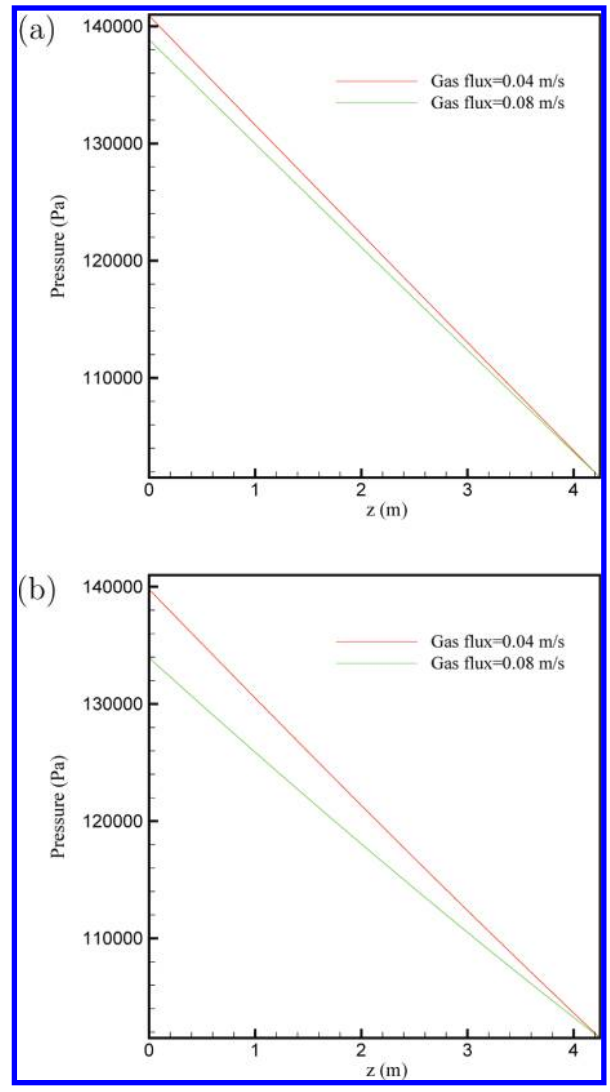

Figure 9. Pressure profile in the axial direction for two different gas flux values, (a) without breakage and coalescence terms, and (b) with breakage and coalescence terms.

experimental data is largest for the upper cross section levels of the channel. In Figure 5a, a large difference between the simulated and averaged experimental data is observed for the highest axial level in the column. The accuracy of the experimental data reported by Jakobsen et al.[27] is questioned as an unsymmetry is occurring in the radial direction as the column probably was inclined. Moreover, the number of measuring points varies for the different measurement series. The data obtained at the additional measuring points represent outlayers, which affect the average values significantly, and hence a particular fixed selection of measuring points was applied in all data series included in the comparison. In Figure 6, the gas area fraction profile predicted with gas flux $j_d = 0.08$ m/s is compared to the corresponding experimental data at channel height 2 m as reported by Jakobsen[28] and at axial level 0.75 and 3.5 m as reported by Yao et al.[31] The results show a good fit with the experimental data.

In Figures 7−10, the effects of bubble coalescence and breakage are evaluated. The first observation made analyzing different simulations is that the impact of coalescence is negligible (the simulated results from the coalescence analysis are not shown due to the article space restrictions), and hence the flow is considered breakage dominant as in most bubble column studies reported in the literature.[4,7,8] Actually, the largest variations in the profiles are due to the bubble gas expansion effects. For α_d, pressure, and density, the lower gas flux profiles are hardly influenced by the breakage terms, whereas for the liquid velocity both profiles have about the same variations. These differences are most likely due to the reduced dissipation rate at the lower gas fluxes. Nevertheless, further investigations are required elucidating the impact of the other mechanisms of bubble coalescence and breakage.[7,8,15,16] Moreover, further validation of the individual kernels is needed, requiring extended well-planned model-based experimental investigations.

Figures 11 and 12 show 3D field plots of the dispersed phase velocity and the mass density function for two different gas fluxes. These profiles seem reasonable, and they fulfill the imposed initial conditions. However, the initial profiles imposed on $v_d(z = 0,\xi)$ and $f_d(z = 0,\xi)$ are approximated on the basis of intuition and very few experimental data. Further experimental work is required to provide sufficient data for a more detailed model validation.

5. Conclusion

A steady-state model for the gas−liquid flow in a bubble column has been solved numerically by the least-squares spectral

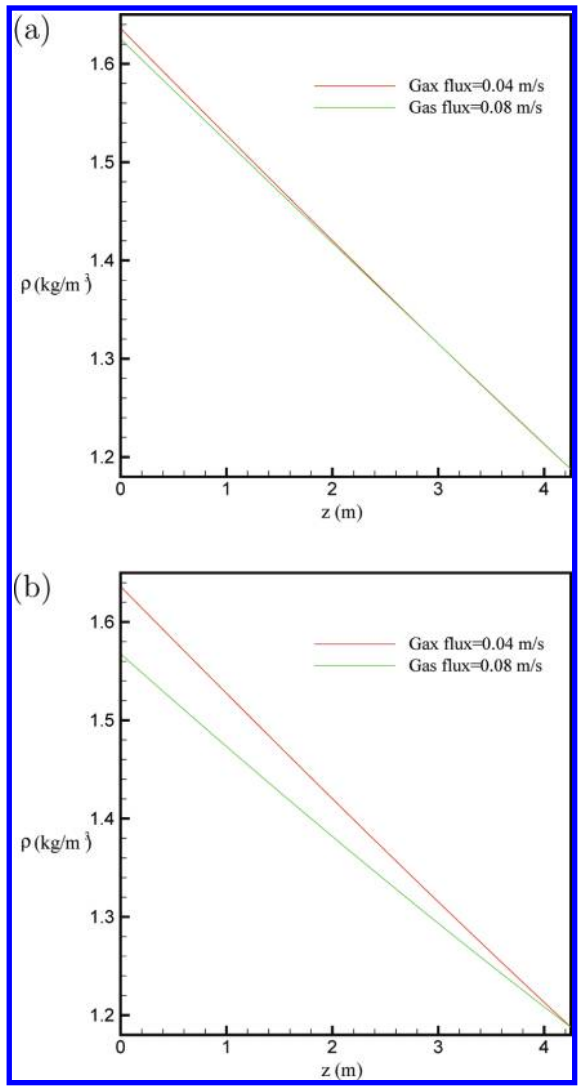

Figure 10. Density variation in the axial direction for two different gas flux values, (a) without breakage and coalescence terms, and (b) with breakage and coalescence terms.

method. The nonlinear terms in the system of equations have been linearized using the Pichard technique, and successive iterations have been applied to obtain a converged solution.

The predicted results have been compared to experimental data found in the literature. The agreement between the measured data and the simulated results is good. Moreover, the predicted results show that the breakage rate significantly influences the behavior of the fully developed flow, whereas the coalescence rate effects are negligible. However, the growth term induces the largest axial variations in the density function, whereas the breakage shifts the distribution toward smaller bubble sizes. Nevertheless, the axial variations of the Sauter mean diameter are small in particular for higher gas holdups.

With access to extensive experimental data on the bubble size distribution, the novel model may be used elucidating the physical relevance of the existing coalescence and breakage kernels. In particular, for the breakage terms, the average number of daughter bubbles created in each breakage event and the basic shape of the redistribution function h_b must be validated. The novel model also allows for an investigation of the bubble number or mass density function given as a function of size and location, and hence this variable must be considered in future experimental studies as little experimental data have been

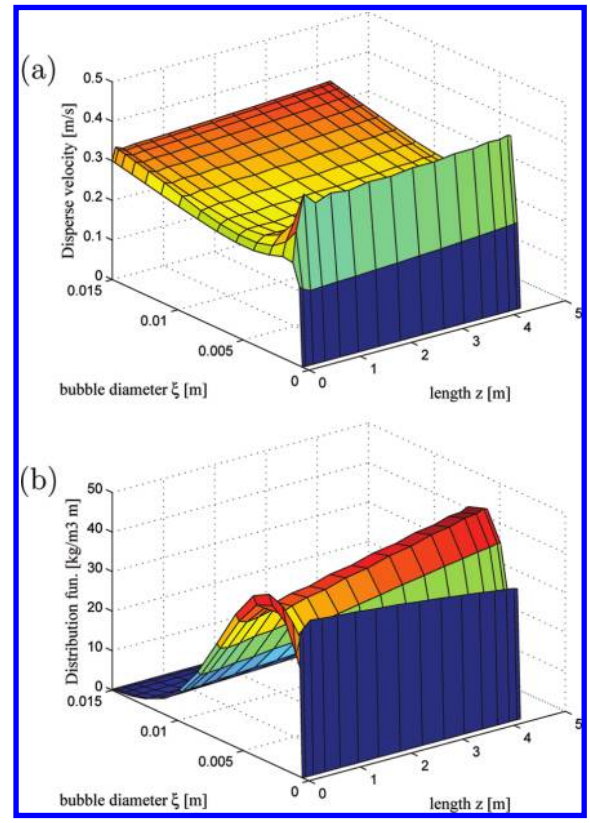

Figure 11. Three-dimensional plots of model results for gas flux $j_d = 0.08$ m/s with breakage and coalescence terms: (a) disperse phase velocity profile, and (b) distribution function profile.

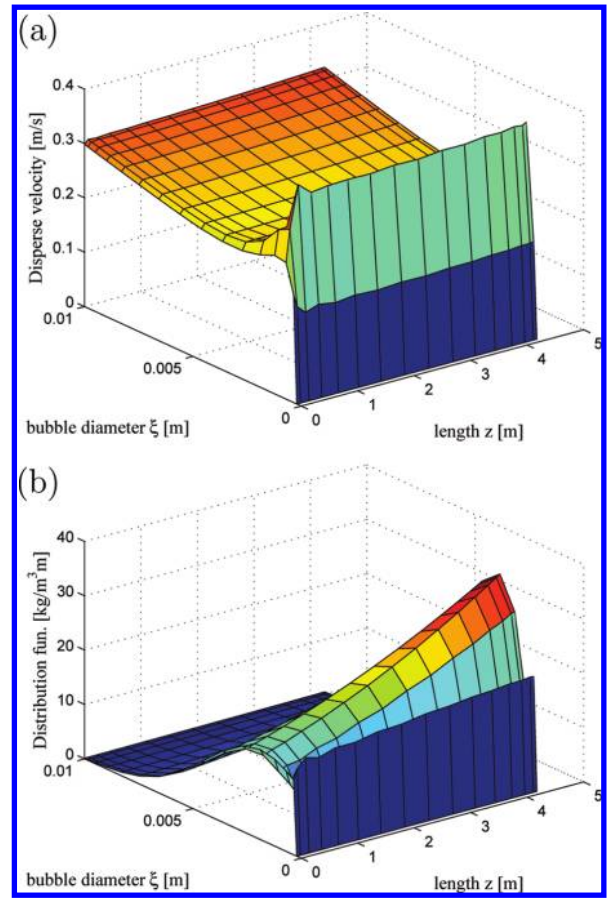

Figure 12. Three-dimensional plots of model results for gas flux $j_d = 0.04$ m/s with breakage and coalescence terms: (a) disperse phase velocity profile, and (b) distribution function profile.

reported in the literature. With such data available, the novel model may assist improving the physical understanding of the pertinent breakage and coalescence mechanisms. One may then develop better mechanistic kernel functions and enable proper fitting of the coalescence and breakage kernel parameters to the experimental data, resulting in more reliable model predictions.

Acknowledgment

The Postdoc fellowship (A.K.N.) and the Ph.D. fellowships (Z.B. and F.S.) financed by the Research Council of Norway through the GASSMAKS programme are highly appreciated.

Notations

A = area under $\phi(\xi)$-curve
$\mathbf{a}$ = generalized coordinate vector for $\mathbf{c}$ and Ξ
$b(\mathbf{r},\xi,t)$ = breakage rate (1/s)
$\mathscr{B}(\mathbf{r},\xi,t)$ = net breakage operator
$\mathscr{B}_0$ = boundary condition operator
$\mathbf{c}$ = velocity in spatial coordinates (m/s)
$c(\mathbf{r},\xi,\zeta,t)$ = coalescence rate (1/s)
$(\mathbf{r},\xi,t)$ = net coalescence operator
C_D = drag force coefficient (−)
D = column diameter (m)
$(D_a())/(D_at)$ = short hand mathematical operator
$d_{32}(\mathbf{r},t)$ = Sauter mean diameter (m)
E_0 = Eötvös number (−)
$\mathbf{F}(\mathbf{r},\xi,t)$ = force vector (N/kg)
$\mathbf{F}_r(\mathbf{r},\xi,t)$ = force vector in physical space (N/kg)
$\mathbf{F}_\xi(\mathbf{r},\xi,t)$ = force vector in the inner coordinate space (N/kg)
$f(\mathbf{q},t)$ = generalized number density
$f(\mathbf{r},\xi,t)$ = number density function (lb/m^3·m)
$f_d(\mathbf{r},\xi,t)$ = mass density function (kg/m^3·m)
$f_{drag}(\mathbf{r},\xi,t)$ = drag force (N/m^3·m)
$f_w(z)$ = wall friction coefficient (−)
g = gravitational acceleration (m/s^2)
g^* = linearized source vector
$h_b(\zeta,\xi)$ = daughter size redistribution function (1/m)
$h_c(\zeta,\xi)$ = swept volume rate (m^3/s)
h_0 = initial film thickness (m)
h_f = critical film thickness for rapture (m)
$J(\psi)$ = generalized source term considering both collisional and noncollisional phenomena
j_d = gas volume flux (m^3/s)
j_l = liquid volume flux (m^3/s)
k_1 = breakage kernel parameter (s)
k_2 = breakage kernel parameter (−)
$\mathscr{L}_B$ = breakage operator
$\mathscr{L}_C$ = coalescence operator
$\mathscr{L}$ = linear problem definition operator
M = molecular weight of air (kg/kmol)
$\dot{M}_{momentum}(z,\xi)$ = momentum flux in ξ-dimension ((kg·m)/(s)/m^3·s)
$\dot{m}_{mass}(z,\xi)$ = mass flux in ξ-dimension (kg/m^3·s)
$m(\mathbf{r},\xi,t)$ = fluid particle mass (kg)
$p(\mathbf{r},t)$ = pressure (Pa)
$p(\mathbf{q},\mathbf{a},t)$ = probability density function
$((\partial p)/(\partial t))_{collisions}$ = generalized source term due to collisions between the entities
$\mathbf{q}$ = generalized coordinate vector for $\mathbf{r}$ and ξ
R = gas constant (J/K·kmol)
Re = Reynolds number (−)
$r_c(\xi,\zeta)$ = equivalent radius (m)
$\mathbf{r}$ = coordinate in physical space (m)
S = generalized source term, independent of the collisions
T = temperature (K)
t = time (s)
$V(\xi) = (4/3)\pi\xi^3$ = volume of bubble (m^3)
$\mathbf{v}(\mathbf{q},t)$ = Maxwellian average velocity (m/s)
$\mathbf{v}_d(\mathbf{r},t)$ = mean gas-phase velocity (m/s)
$v_{d,slip}(\xi)$ = slip velocity (m/s)
$v_l(z)$ = liquid-phase velocity (m/s)
$\mathbf{v}_r(\mathbf{r},\xi,t)$ = gas-phase size-dependent velocity (m/s)
$\overline{v_t^2}(\xi)$ = Kolmogorov structure function, a two-point velocity correlation (m^2/s^2)
$\mathbf{v}_\xi$ = growth velocity (m/s)
z = axial coordinate (m)

Greek Letters

α_l = liquid area fraction (−)
α_d = gas area fraction (−)
β = parameter in statistical turbulence theory (−)
ε = turbulent kinetic energy dissipation rate per unit mass (m^2/s^3)
ε_{L2} = residual error measure (−)
$\varepsilon_{iteration}$ = iteration error measure (−)
μ_l = liquid dynamic viscosity (kg/ms)
μ_d = gas dynamic viscosity (kg/ms)
σ_l = gas−liquid surface tension (N/m)
ρ_l = liquid density (kg/m^3)
ρ_d = gas density (kg/m^3)
ζ = bubble diameter (m)
ξ = generalized coordinate in property space or bubble diameter (m)
Ξ = velocity in the internal coordinate (m/s)
ξ_{max} = maximum bubble diameter (m)
ξ_{min} = minimum bubble diameter (m)
Ω = computational domain
$\psi(\mathbf{q},\mathbf{a},t)$ = generalized property
∇ = nabla operator
Γ = computational boundary domain, or gamma function
$\lambda_c(\xi,\zeta)$ = coalescence probability (−)
$\phi(\xi)$ = Gaussian distribution function (1/m)
$\langle\cdots\rangle_M$ = Maxwellian average operator

Literature Cited

(1) Shah, Y.; Kelkar, B.; Godbole, S.; Deckwert, W. Design parameters estimations for bubble column reactor. *AIChE J.* **1982**, *28*, 353–379.

(2) Dorao, C. A.; Jakobsen, H. A. A least squares method for the solution of population balance problems. *Comput. Chem. Eng.* **2006**, *30*, 535–547.

(3) Dorao, C. A.; Jakobsen, H. A. Least-squares spectral method for solving advective population balance problems. *J. Comput. Appl. Math.* **2007**, *201*, 247–257.

(4) Zhu, Z.; Dorao, C. A.; Lucas, D.; Jakobsen, H. A. On the coupled solution of a combined population balance model using the least-squares spectral element method. *Ind. Eng. Chem. Res.* **2009**, *48*, 7994–8006.

(5) Patruno, L. E.; Dorao, C. A.; Dupuy, P. M.; Svendsen, H. F.; Jakobsen, H. A. Identification of droplet breakage kernel for population balance modelling. *Chem. Eng. Sci.* **2009**, *64*, 638–645.

(6) Patruno, L. E. Experimental and Numerical Investigations of Liquid Fragmentation and Droplet Generation for Gas Processing at High Pressures. Thesis, NTNU, Trondheim, Norway, 2010.

(7) Jakobsen, H. A.; Lindborg, H.; Dorao, C. A. Modelling of bubble column reactors: progress and limitations. *Ind. Eng. Chem. Res.* **2005**, *44*, 5107–5151.

(8) Jakobsen, H. A. *Chemical Reactor Modeling: Multiphase Reactive Flows*; Springer: Berlin, Germany, 2008.

(9) Lafi, A. Y.; Reyes, J. N. *General Particle Transport Equation. Final Report. OSU-NE9409*; Department of Nuclear Engineering, Oregon State University: Oregon, 1994.

(10) Lasheras, J. C.; Eastwood, C.; Martinez-Bazan, C.; Montanes, J. L. A review of statistical models for the break-up of an immiscible fluid immersed into a fully developed turbulent flow. *Int. J. Multiphase Flow* **2002**, *28*, 247–278.

(11) Lathouwers, D.; Bellan, J. Yield optimization and scaling of fluidized beds for tar production from biomass. *Energy Fuels* **2001**, *15*, 1247–1262.

(12) Morel, C.; Ruyer, P.; Seiler, N.; Laviéville, J. M. Comparison of several models for multi-size bubbly flows on an adiabatic experiment. *Int. J. Multiphase Flow* **2010**, *36*, 25–39.

(13) Ramkrishna, D. *Population Balance: Theory and Applications to Particulate Systems in Engineering*; Academic Press: San Diego, CA, 2000.

(14) Berman, S. M. J. *Mathematical Statistics: An Introduction Based on the Normal Distribution*; PA: In text Educational Publishers: 1971.

(15) Liao, Y.; Lucas, D. A literature review of theoretical models for drop and bubble breakup in turbulent dispersions. *Chem. Eng. Sci.* **2009**, *64*, 3389–3406.

(16) Liao, Y.; Lucas, D. A literature review on mechanisms and models for the coalescence process of fluid particles. *Chem. Eng. Sci.* **2010**, *65*, 2851–2864.

(17) Dorao, C. A.; Jakobsen, H. A. Time-space-property least squares spectral method for population balance problems. *Chem. Eng. Sci.* **2006**, *62*, 1323–1333.

(18) Tomiyama, A. Struggle with computational bubble dynamics. *Third International conference on Multiphase Flow*; Lyon, France, June 8−12, 1998.

(19) Coulaloglou, C. A.; Tavlarides, L. L. Description of interaction processes in agitated liquid−liquid dispersions. *Chem. Eng. Sci.* **1977**, *32*, 1289–1297.

(20) White, F. M. *Fluid Mechanics*; McGraw-Hill Book Co.: Columbus, OH, 1979.

(21) Konno, M.; Aoki, M.; Saito, S. Scale effect on break-up process in liquid-liquid agitated tanks. *J. Chem. Eng. Jpn.* **1983**, *16*, 312–319.

(22) Prince, M. J.; Blanch, H. W. Bubble coalescence and break-up in air-sparged bubble column. *AIChE J.* **1990**, *36*, 1485–1499.

(23) Fan, L. S.; Tsuchiya, K. *Bubble Wake Dynamics in Liquids and Liquid−Solid Suspensions*; Butterworth-Heinemann Series in Chemical Engineering: Woburn, MA, 1990.

(24) Jiang, B. *Least-Squares Finite Element Method: Theory and Applications in Computational Fluid Dynamics and Electromagnetics*; Springer: New York, 1998.

(25) Bochev, P. B.; Gunzburger, M. D. *Least-Squares Finite Element Methods, Applied Mathematical Sciences*; Springer: New York, 2009; p 166.

(26) Bhole, M.; Joshi, J.; Ramakrishna, D. CFD simulation of bubble columns incorporating population balance modeling. *Chem. Eng. Sci.* **2008**, *63*, 2267–2282.

(27) Jakobsen, H. A.; Hjarbo, K. W.; Svendsen, H. F. SINTEF Report: STF21 F93103, 1994.

(28) Jakobsen, H. A. On the modelling and simulation of bubble coloumn reactors using a two-fluid model. Thesis NTH, Trondheim, Norway, 1993.

(29) Gasche, H. E. Modellierung von Blasensäulen. Thesis, Erlangen, Germany, 1989.

(30) Grienberger, J. Untersuchung and Modellierung von Blasensäulen. Thesis, Erlangen, Germany, 1990.

(31) Yao, B. P.; Zheng, C.; Gasche, H. E.; Hofmann, H. Bubble behaviour and flow structure of bubble columns. *Chem. Eng. Process.* **1991**, *29*, 65–75.

Received for review August 4, 2010
Revised manuscript received September 24, 2010
Accepted November 26, 2010

IE101664W